COBEM 2023 27TH INTERNATIONAL CONGRESS OF MECHANICAL ENGENEERING

ABCM Brazilian Society of Mechanical Sciences and Engineering
27th ABCM International Congress of Mechanical Engineering
December 04-08, 2023, Florianópolis-SC, Brazil

COB-2023-0607
EXPERIMENTAL ANALYSIS OF A SMART SOFT BEAM ACTUATED BY SMA THIN RIBBON ACTUATORS

Antonio Cláudio Cavalcanti Holanda
Federal University of Paraíba (UFPB), Campus I, Cidade Universitária, ZIP code 58051-900, João Pessoa – PB, Brazil
antonio.c.holanda@hotmail.com

Carlos José de Araújo
Federal University of Campina Grande (UFCG) - Av. Aprígio Veloso, 882 – Bairro Universitário, Zip Code: 58429-140, Campina Grande – PB, Brazil.
carlos.jose@professor.ufcg.edu.br

Cícero da Rocha Souto
Federal University of Paraíba (UFPB), Campus I, Cidade Universitária, ZIP code 58051-900, João Pessoa – PB, Brazil
cicerosouto@cear.ufpb.br

Abstract. *In the field of intelligent structures, researchers are always searching for new combinations of intelligent materials with other materials in order to achieve specific characteristics and innovative applications. Shape Memory Alloys (SMA) is one such material that offers a wide range of applications due to its unique characteristics, particularly when combined with soft polymer matrices. Smart structures made using these materials can be designed to produce various movements, making them suitable for use in actuators, adaptive structures, and soft robots. Additionally, SMA-based actuators are more compact, lighter, and quieter than traditional actuators. This study proposes the development of a soft beam activated by SMA ribbons embedded in a soft silicone matrix and fixed in an ABS polymer structure. The beam bends when the SMA ribbons are activated by an electric current. The study was divided into two main phases: the first phase involved obtaining and characterizing the thermomechanical properties of the SMA ribbons, while the second phase focused on the design, manufacture, and testing of the soft beam activated by the embedded SMA ribbons. The beam underwent drive, blocking force, and deformation tests, and the results showed that it reached a maximum deflection value of approximately 72.0 mm at the free end and a maximum rotation angle of 27.5º during an activation time of 30 seconds. The maximum blocking force observed was 0.8 N for a minimum distance of 0 mm and 0.25 N for a distance of 20 mm from a blocking plate. Based on these results, it can be concluded that the presented soft beam concept offers a good alternative to traditional actuators commonly used in robotic grippers, biomimetic actuation modules, and adaptive aerodynamic structures.*

Keywords: *Shape memory alloys, Smart soft structures, Soft beam, NiTi SMA ribbons.*

1. INTRODUCTION

The expansion in the researches concerning composite materials due to their intrinsic properties, coupled with significant advancements in the development of increasingly efficient sensors and actuators, has led to the emergence of smart composites. These composites differ from traditional ones by possessing adaptive behaviors that allow greater functionality and flexibility of properties. These smart composites can effectively adapt to varying loads and environmental changes, modifying their response to overcome specific conditions (Wei *et al*., 1998).

In this context, composite structures based on shape memory alloys (SMA) are being increasingly investigated. These alloys possess unique thermomechanical properties that, when combined with other structural materials, enable the development of a wide range of smart composites (De Araújo *et al*., 2008). Among these, composites with polymeric matrices represent a promising technological opportunity and an alternative solution to conventional mechanical systems, allowing the development of simple, compact, and reliable mechanisms (Cohades and Michaud, 2018).

The application of soft matrices in these smart structures has shown promising potential for actuator development. The ability to modify the geometry of such composites enables the production of various movements, including bending, twisting, bending-torsion, and even more complex movements found in nature (Rodrigue *et al*., 2015). The concept designs range from underwater robotic structures (Kazemi Lari *et al*., 2019) to hand and gripper prototypes (Lee *et al*., 2019; Wang *et al*. 2020), soft morphing skins (Han *et al*., 2020) and biomimetic structures that aim to emulate the movements of highly soft animals (Almubarak *et al.,* 2020).

Recently, Tsimbo Fokou *et al*. (2023) proposed a Soft Robotic Fish actuated by artificial muscle composed by actuators based on SMA wires. Hwang and Wang (2022) developed a flexible amphibious robot with the capability to generate

multimodal terrestrial and subaqueous motion, which has not been previously demonstrated by other SMA-based flexible robots. Zheng *et al*. (2022), proposed a multifunctional flexible actuator composed of NiTi wires embedded and untethered, activated by infrared. In the field of aerodynamic applications, Khan *et al*. (2021) developed a fin-shaped smart composite for application in ballistic missiles.

Some applications of SMA actuators have been focusing on the development of soft structures applied in wearable devices, where SMA wires are woven into textile meshes to produce compression clothes, orthoses, self-conformable shoes (Granberry *et al*., 2021), movement assistance devices (Park and Park, 2019; Jung et al., 2022) and soft exogloves (Lee *et al*., 2022).

The effectiveness of these structures is linked to the quality of adhesion at the metal/matrix interface, which must have sufficient strength to transmit the stresses and deformations imposed by the SMA actuators. Although the use of NiTi SMA wires is still predominant in such structures, it presents problems related to adhesion (Smith *et al*., 2004). To mitigate this issue, the replacement of NiTi wires by NiTi ribbons emerges as an interesting alternative, as the rectangular geometry of the ribbons offers a larger contact area with the matrix.

Therefore, this experimental work aims to analyze a soft smart beam activated by embedded NiTi ribbons into a soft silicone matrix, fixed in a 3D printed ABS polymer structure. The SMA ribbons are activated by electric current and undergo deformation through the two-way shape memory effect (TWSME), resulting in a bending movement of the structure.

The methodology applied in this work was divided into two main stages. The first involved the manufacturing and preparation of the actuators (NiTi ribbons), followed by thermomechanical characterization. In the second stage, the concept of the soft beam was developed, the structure was fabricated, and activation tests were performed to measure the blocking force generated and the geometry variation induced by actuator deformation inside the beam.

1.1 Shape memory alloy actuators

Shape memory alloys (SMA) are special metallic materials that can recover a considerable deformation introduced at a low temperature through subsequent heating above a critical temperature, exhibiting a minimum residual deformation. This characteristic is related to the ability of these materials to undergo phase transformations in the presence of applied mechanical stress and/or temperature variations. This transformation occurs between two crystalline structures, austenite and martensite. Austenite is the phase present at higher temperatures and has greater stiffness, while martensite occurs at lower temperatures and is easily deformable (Lagoudas, 2008).

All these transformations occur at characteristic temperatures: M_s (martensitic start), M_f (martensitic finish), A_s (austenitic start), and A_f (austenitic finish). Based on these crystallographic mechanisms, the phenomenon of Shape Memory Effect (SME) occurs, as represented in Figure 1 for SME (a) and TWSME (b).

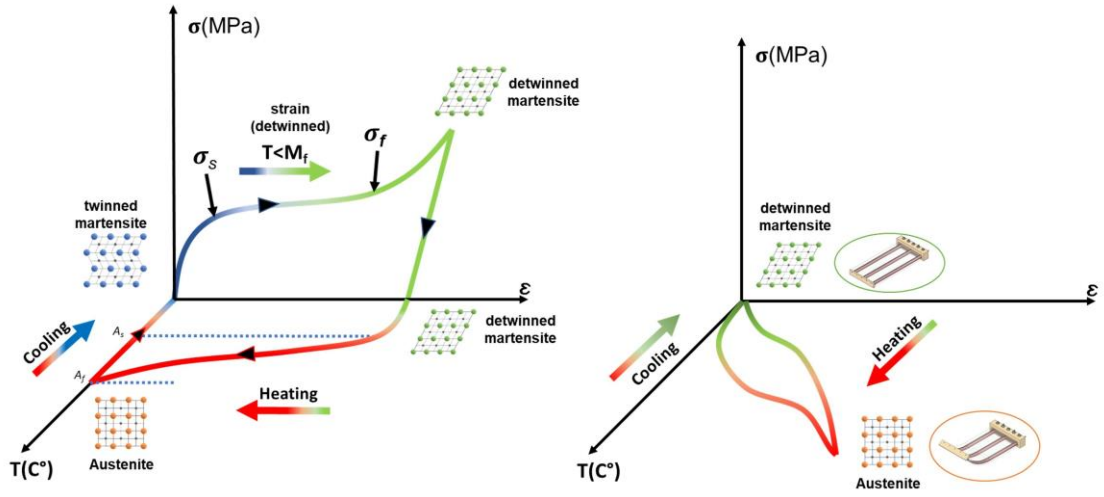

(a) (b)

Figure 1. Thermomechanical cycle for SME (a) and TWSME (b) in shape memory alloys (Adapted from Lagoudas, 2008).

The shape memory effect (SME, a) occurs when a SMA recover its initial shape, after a pseudoelastic deformation introduced at low temperature, only by increasing the temperature (heating). In the condition of twinned martensite, the SMA undergoes deformation by an applied stress and changes to detwinned martensite. A significant portion of this deformation remains after unloading. However, upon subjecting the SMA to an increase in temperature above A_f, the material recovers this deformation (Otsuka and Wayman, 1998). When the SMA is able to "memorize" its shape at both

low and high temperatures, it is said to have a Two-Way Shape Memory Effect (TWSME), as represented in Figure 1(b). This phenomenon allows the material to change between the two shapes simply by changing the temperature, without the need for applied load (Antonucci and Martone, 2015). The TWSME behavior (Fig. 1b) can be obtained after some cycles in SME mode (Figure 1a), in a procedure called "training" (Otsuka & Wayman, 1998).

Due to these characteristics, the development of actuators using SMAs becomes highly attractive in various fields of engineering, particularly for replacing conventional actuators that are heavy, noisy, such as motors and solenoid valves (Kohl, 2004).

In a recent study, Kim *et al*. (2023) presented a discussion about the development of SMA actuators in recent years. The wide range of technologies available today allows SMA-based actuator systems to be adapted in terms of material, shape and scale. It is therefore possible to select the shape of these materials according to a specific deformation to be achieved and the complexity of the movements, as well as taking advantage of these characteristics to manufacture independent actuators, soft composites or textile composites. In the field of Smart Soft Composites, the type of motion and amplitude will be crucial for the composition of the actuator, which may include SMA components, scaffolds, matrices of different stiffness and even textile meshes.

2. MATERIALS AND METHODS

2.1 Manufacture and thermomechanical characterization of SMA ribbons

The SMA ribbons were produced by a cold rolling from a NiTi SMA wire of 0.29mm in diameter, involving two steps. The first pass imposed a 25% reduction in the wire's cross-sectional area, while the second pass reduced it by 60%. The maximum reduction was limited at 70%, as suggested by Demers *et al*. (2009) to avoid the loss of desired properties. The final cross-section dimensions of the ribbon were 0.64mm in width and 0.08mm in thickness.

After rolling, the as processed ribbon was submitted to an annealing heat treatment for 20 minutes at 400°C, followed by air cooling. This treatment aimed to eliminate the effects of work hardening caused by the cold rolling process and achieve the SME. Subsequently, a thermal analysis was performed to determine the transformation temperatures of the SMA ribbon. A differential scanning calorimetry (DSC) test was conducted for this purpose and Figure 2 shows the obtained DSC graph. By applying the tangent method, the transformation temperatures of the NiTi ribbon were determined.

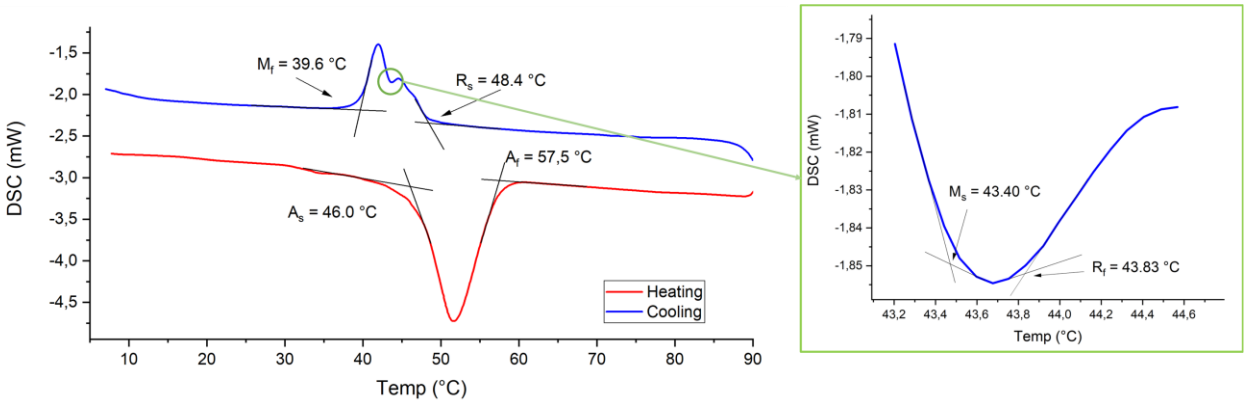

Figure 2. Transformation temperatures of the NiTi SMA ribbon obtained by DSC.

The ribbon exhibited a two-step transformation involving R-phase during cooling due to the mechanical processing. The M_f temperature of 39.6°C indicates that the component is in the martensitic state at room temperature while A_f of 57.5ºC indicates that SME can be observed after deformation below M_f and heating above this temperature.

The mechanical characterization of the ribbon was performed through a uniaxial tensile testing at room temperature (23°C). Figure 3 shows the setup of the tensile test and the stress-strain curve obtained. From this result, it is possible to determine the initial stress value at which martensite begins its orientation (σ_s= 50 MPa) and the final stress (σ_f = 80 MPa), which determines the end of the orientation plateau.

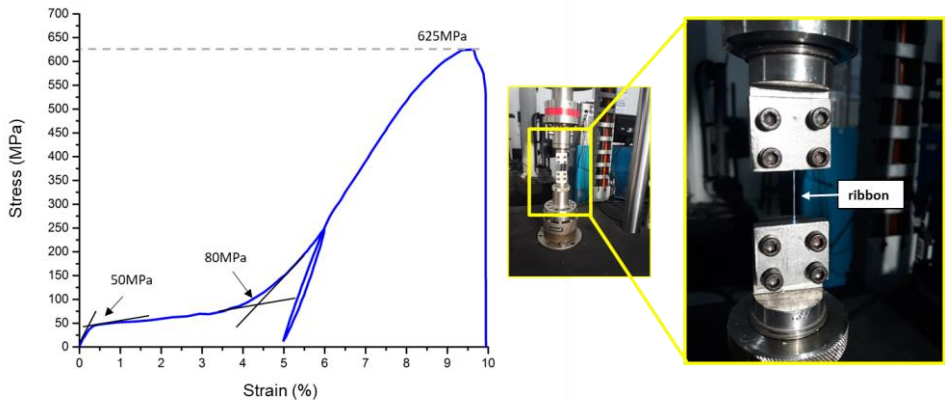

Figure 3. Stress vs strain for the obtained NiTi ribbon.

After loading up to 6% deformation, the ribbon was unloaded, resulting in a residual deformation of 5%, which could be recovered upon heating above A_f. The tensile strength was 625 MPa, reaching a deformation of approximately 10% before fracture. These values can be explained by the improvement in the tensile properties of NiTi alloys in the rolling direction, causing material anisotropy and microstructural evolution (Sharifi *et al*., 2014).

2.2 Thermomechanical training and recovery test of SMA ribbons

After the thermal and mechanical characterizations, the SMA ribbon actuator was subjected to thermomechanical cycling training to achieve the TWSME. Since deformation recovery in the longitudinal direction is required, the ribbon was vertically fixed with uniaxial loading applied at one end (dead weight). The cycling was performed at room temperature (23°C), where the actuator is in the martensitic phase (M_f = 39.6°C). The applied load was 10.24N, sufficient to generate a tensile stress of the order of σ_f = 80MPa and ensure that the martensite microstructure is fully detwinned.

The ribbon actuator was heated by Joule heating to recover the deformation, using cyclic passage of electric current with the aid of an adjustable DC power supply and a control circuit. The cycle consists of activation time (current passage) followed by return time (cooling) of the ribbon. At the end of each cycle, a portion of the deformation remains after heating. As the number of cycles increases, this accumulation of deformation decreases until saturation is reached, where all deformation is recovered through heating.

Therefore, to stabilize the SMA ribbon deformation, 500 cycles of heating followed by cooling at room temperature under constant load were employed. Figure 4 illustrates the training setup and the parameters used.

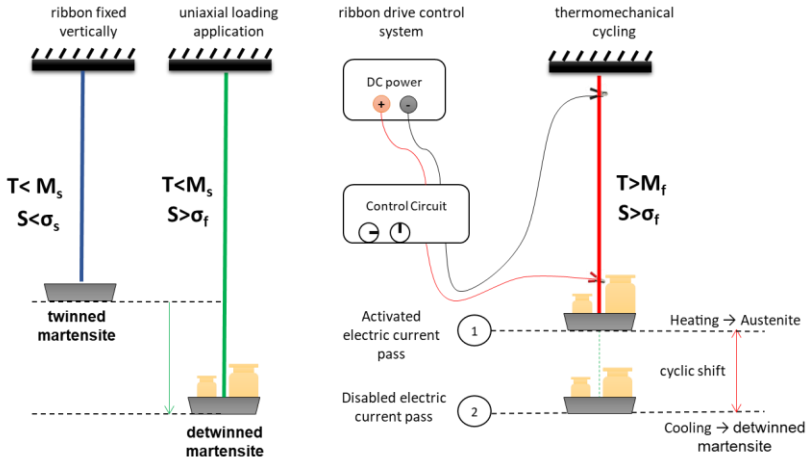

Training parameters	
Cross-sectional area	0.051 mm²
Final stress (sf)	120 MPa
Af	57.5 °C
Load	10.24 N
Applied mass	1.24 kg
Current	0.8 A
cycle length	30 s
number of cycles	500
Recovery after stabilization	3.5%

Figure 4. Thermomechanical training and parameters.

The current supplied by the DC power supply was regulated until the full shape recovery of the ribbon was observed. Using a K-type thermocouple (100µm in diameter) attached to the surface of the ribbon, the temperature variation during activation was measured. Thus, an electric current of 0.8A was determined, sufficient for the ribbon to reach the A_f temperature without causing overheating, which could lead to the loss of shape memory properties. After completing the process for 500 cycles, it was observed that the ribbon stabilized with a recovery of approximately 3.5%.

The potential for generating mechanical load by the SMA ribbon through the TWSME was evaluated through load recovery tests. The trained ribbon was cut into 100mm lengths, corresponding to the useful size of the actuators applied to the soft beam. The sample was then fixed and pre-tensioned to a load of 0.5N and activated by the current defined during the training. Figure 5 illustrates the experimental setup employed to obtain the results shown in Figure 6.

Cycling tests carried out by Holanda (2021) on NiTi SMA actuator wires and ribbons showed stabilization on 50 cycles, with low hysteresis variation up to 500 cycles. Miller and Lagoudas (2000) also obtained results indicating stabilization at about 50 thermal cycles on SMA wires under constant stress.

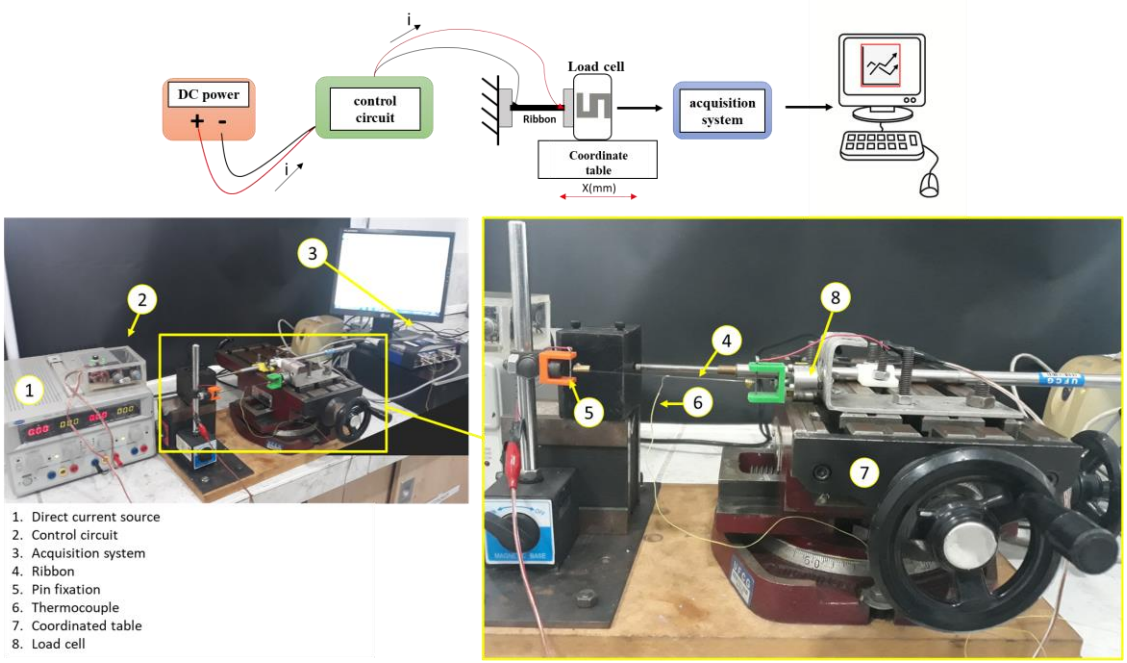

Figure 5. Load recovery test setup.

Figure 6(a) show the behavior of the load generated by each trained NiTi SMA ribbon as a function of time, corresponding to 50 activation cycles. It can be observed that the average loading recovery by the SMA ribbon is of the order of 19.49 ± 1.40 N.

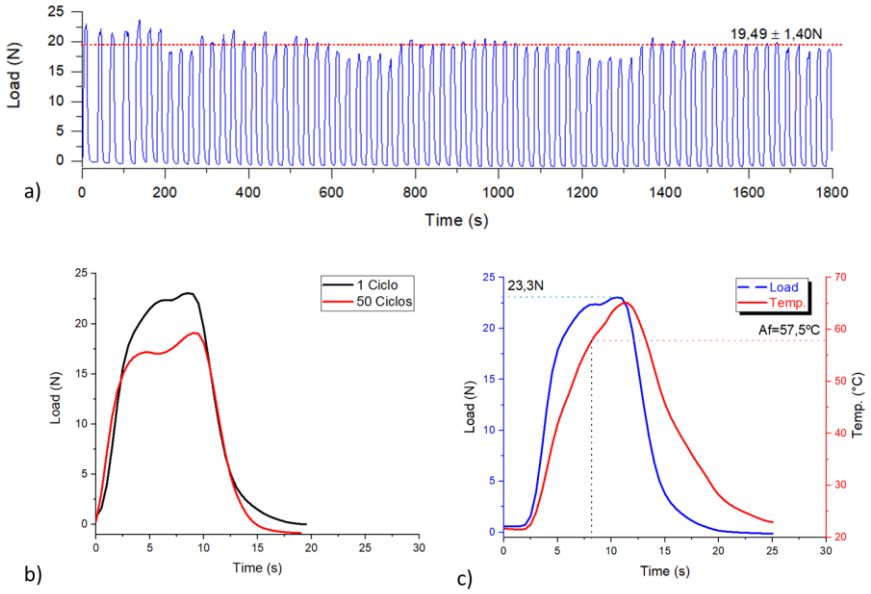

Figure 6. Load recovery as a function of time. (a) Variation of the load generated during 50 activation cycles; (b) Load generated in the first and last cycle; (c) Variation of load and temperature as a function of time in the first activation cycle.

The variable behavior of the force generated throughout the cycling is an intrinsic response of the resistive heating dynamics by electric current pulses. Although a slight reduction in force was observed between the first and last cycles (Figure 6b), this behavior cannot be considered a loss of functionality or functional material fatigue, but it occurs due to the presence of micro displacements and ribbon accommodation in the fastening elements of the experimental setup.

A current of 0.8A allows the ribbon to reach A_f = 57.5°C in about 8s, which is sufficient for the ribbon actuator to fully recover its strain. The current can be increased to enhance the heating rate; however, the activation period must be reduced to prevent overheating of the actuator.

This reduction in the activation period may compromise the efficiency of the ribbon in moving the soft beam, as prematurely ceasing the current flow could result in the beam not completing its movement and initiating the return before reaching its maximum deflection. Therefore, the relationship between electrical current, activation time, and cooling time should be optimized for the system to operate effectively.

2.3 Design and manufacture of a soft beam driven by SMA ribbons

The second stage of this work involved the design of the smart soft beam. The design and its components are illustrated in Figure 7. The initial basic geometry established for the beam was a rectangular block with dimensions of 5 mm in height, 50 mm in width, and 100 mm in length.

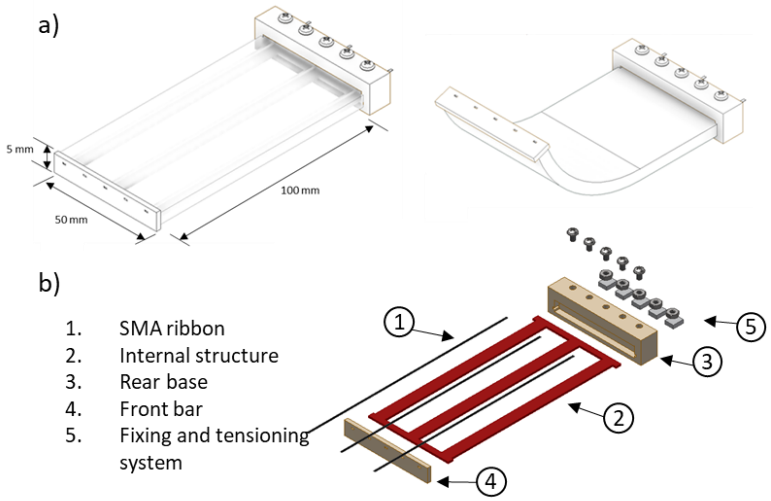

Figure 7. Smart soft beam driven by NiTi SMA ribbon actuators. (a) Soft beam concept. (b) Assembly configuration of the structure's rigid components.

The internal architecture of the soft beam comprises a rigid section consisting of 3D-printed ABS components that form a skeleton, along with three SMA ribbons affixed to its ends. This skeleton features rods measuring 0.5 mm in thickness and 5 mm in width, which are connected to a movable bar at the front end and clamped to a fixed base located at the rear end. A detailed illustration of this configuration can be found in Figure 7(b).

The front bar is designed to be movable and serves the purpose of securing one end of the SMA ribbons. The rear base is an external component and plays an essential role in securing the beam, as it supports the entire internal structure and serves as an anchoring and adjustment point for the ribbons to keep them fully stretched. Additionally, electrical connections for supplying the activating current are established at the rear base.

Following the 3D printing of the structure and mold, the components are assembled and prepared to receive the silicone resin. The skeleton is first positioned parallel to the mold base within the rear base. The SMA ribbons are then affixed to the front end and clamped end, with screw tensioners employed to maintain the desired tautness. The ribbons are aligned in parallel with the skeleton rods, positioned 2.0 mm from the beam's neutral axis and 4.0 mm from the skeleton.

Upon completion of the structure assembly and its fixation within the mold, the silicone resin is prepared and poured into the mold to vulcanization. The chosen matrix material for this process is Silpuran 2420 A/B, a silicone rubber with excellent fluidity, low viscosity, and vulcanization at room temperature. The configuration for receiving the silicone resin, along with the final manufactured beam, is depicted in Figure 8.

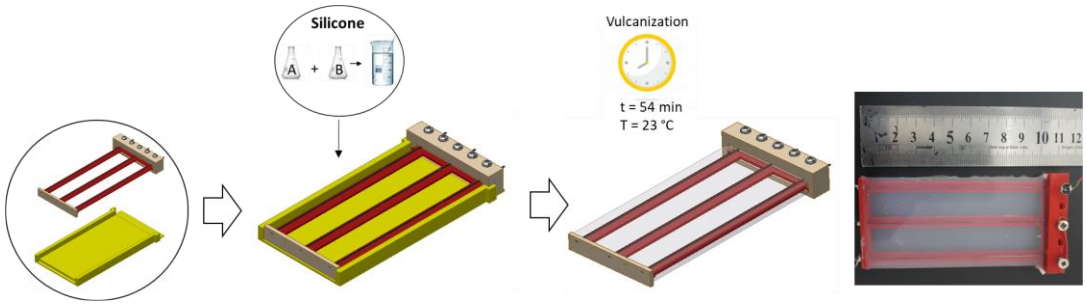

Figure 8. Assembly of the structure in the mold to receive the silicone and obtain the smart soft beam after the silicone has cured.

3. RESULTS AND DISCUSSIONS

In this section, all results obtained with the smart soft beam will be presented and discussed.

3.1 Blocking force test

The blocking force test allow the assessment of the maximum force generated by the soft beam actuator when in contact with a surface. As the title suggests, it refers to the force required to block the actuator's action. These data are crucial for evaluating the potential applications of the device and its limitations regarding load generation. The actuator was positioned vertically and activated against a load cell, as shown in Figure 9.

The maximum force generated was measured as a function of the distance gap between the beam's end and the blocking point (X(mm) in Figure 9a). The analyzed distances were 0, 5, 10, 15, and 20 mm, and the obtained results are presented in Figures 9(b) and 9(c), depicting the variation of force over the activation time and the maximum blocking force generated for each gap.

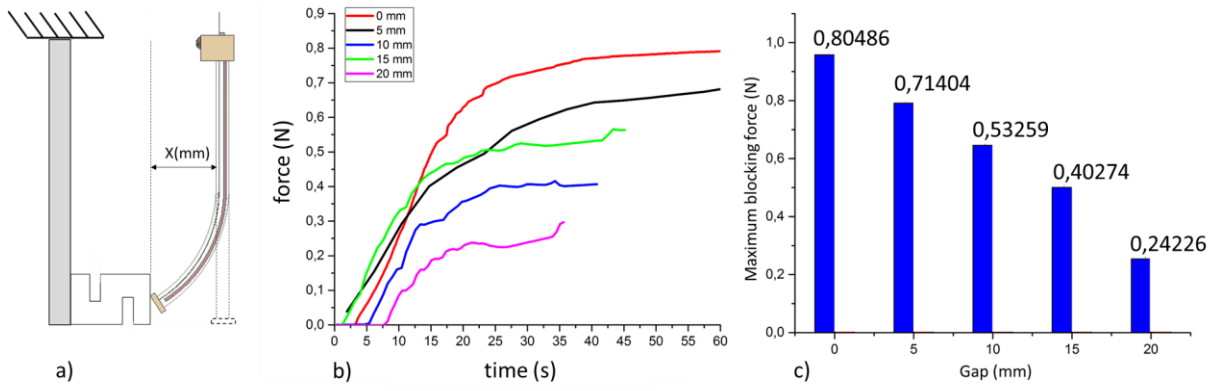

Figure 9. Load generation using the smart soft beam. (a) Blocking force test configuration. (b) Variation of force as a function of time for each gap X(mm). (c) Maximum force values for each analyzed gap.

A approximately linear decrease in the blocking force values is observed with an increase in the gap distance, as pointed out in Figure 9(c). The activated beam exhibits a rapid initial force increase until it stabilizes and reaches its maximum force. The highest load occurs at the zero gap, where a force of 0.80N was obtained, while at the 20mm gap, the force decreased to 0.24N. These values are satisfactory when compared to blocking force tests presented in previous studies, such as those realized by Smith *et al.* (2011) and Wu *et al.* (2013), where the values did not exceed 0.06N for a 0mm gap.

3.2 Free deflection tests

The deflection analysis of the soft beam activated by SMA ribbons was carried out using image analysis, allowing for the evaluation of geometry changes, actuation speed, rotation angle, and maximum deflection. Since the beam was designed for activation by up to 3 ribbons, three activation possibilities were analyzed: using activation of one, two, or three ribbons simultaneously.

The smart soft beam was activated until reaching maximum deflection, and thus the electrical current was maintained until the bending motion of the structure no longer progressed, as indicated by the images of Figure 10. Figure 10 shows

the final positions of the soft beam for the three activation possibilities. For the activation times, were considered the instants of current application initiation and the end of maximum deflection, estimated from the images obtained by recording the beam. A pulse of electric current of 0.8A was applied.

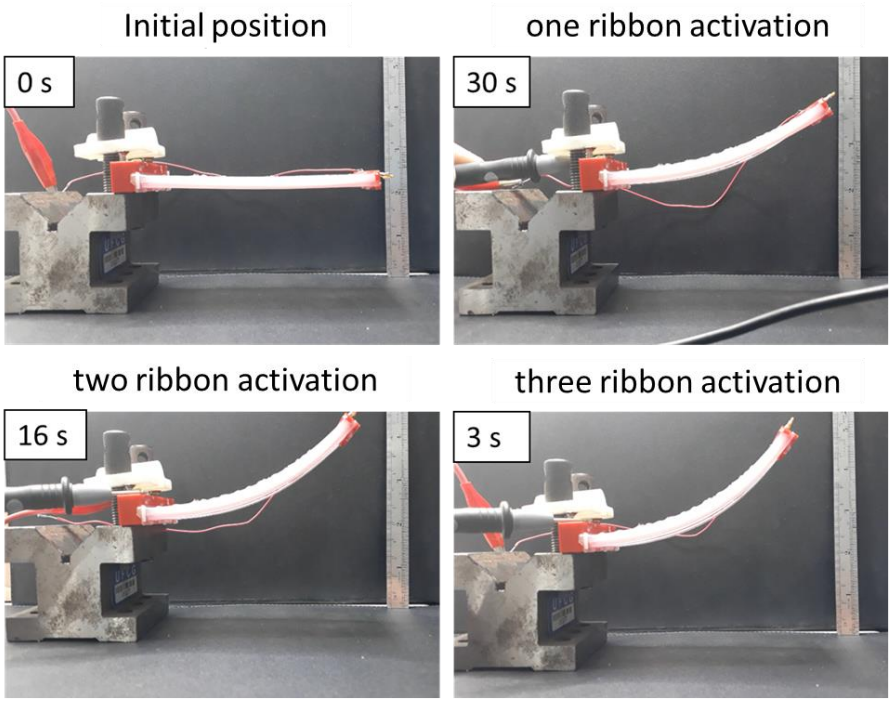

Figure 10. Final position of the beam and activation time for each proposed configuration activated using 0.8A.

This deflection movement is the result of the combination between the 3.5% longitudinal recovery of the ribbon by TWSME and the moment generated by its positioning relative to the beam's neutral axis, causing the desired bending of the structure. The rotation angle θ and deflection y of the free end of the beam were estimated through image analysis, as shown in Figure 11. The rotation angle is measured between the tangent line with respect to the free end and the longitudinal axis, while the deflection consists of the measurement of displacement along the vertical axis. The obtained values are presented in Table 1.

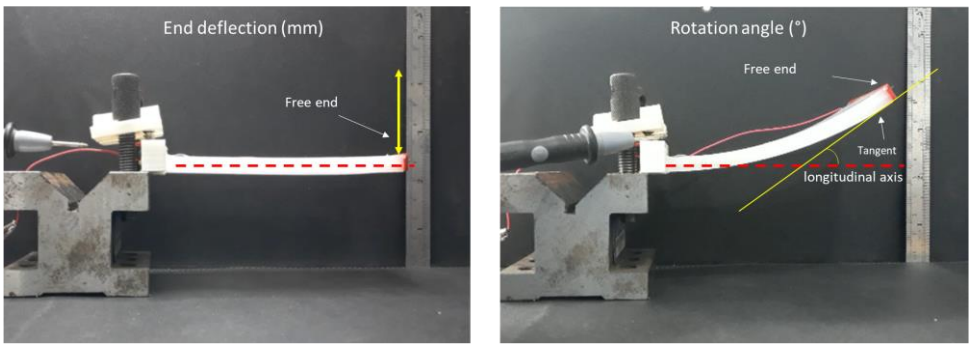

Figure 11. Deflection and rotation angle measurement via image analysis.

Table 1. Deflection test results.

Number of Activated Ribbons	**1**	**2**	**3**
Rotation Angle θ(°)	18.2	23.8	27.5
Deflection y (mm)	35	60	72
Activation time (s)	30	16	3

As expected, the activation of all 3 ribbons resulted in the highest deflection values (72mm) and rotation angle (27.5°), as well as the shortest activation time of 3 seconds. Based on these results, it can be observed that increasing the number of actuator ribbons tends to increase the activation frequency of the structure without the need to increase the current intensity.

4. CONCLUSIONS

In this work, a concept design of a smart soft beam activated by NiTi SMA ribbons was experimentally analyzed. The study aimed to involve the manufacturing of the SMA actuator and its characterization, as well as its application in a soft composite beam. Finally, the behavior of the beam in motion was evaluated.

The manufacturing process of the NiTi ribbons proved to be of utmost importance for the results, as changes in cold rolling parameters or heat treatment significantly influence the efficiency of the actuators. The use of abrupt cold rolling passes (50 to 60%) enabled the attainment of good SME characteristics and mechanical strength without compromising the integrity of the actuator. The recoverable deformation by TWME of 3.5% and the load recovery of 23.5N observed in the load test provide the actuator with a good power density. This results in a considerable power per unit volume compared to conventional actuators, making SMA ribbons a good alternative for compact systems.

The proposed concept design proved to be easy to manufacture and offered a range of possibilities for variations in configuration, such as changes in dimensions, geometry, and even the positioning of the SMA ribbons to achieve different behaviors. The position of the ribbon relative to the rigid structure and the neutral axis of the beam is crucial for the final deflection obtained. In the blocking force tests, the maximum force of 0.8N at zero gap and 0.2N at a 20mm gap should be considered in the applications of this structure. If an application in grips or clamps is desired, the maximum contact force and its variation with increasing gap will determine the type and limit of the load to be manipulated.

As observed, an increase in the number of SMA ribbon actuators increased the maximum deflection of the beam and its actuation speed, reaching 72mm in 3 seconds. Therefore, it is an interesting alternative when aiming to increase the actuation speed of the beam, as increasing the current intensity can overheat the actuators and lead to a loss of memory properties, as well as slow down the cooling and return of the actuator.

Finally, the smart beam concept design studied in this work presents itself as a good alternative to soft actuators commonly found in the literature, typically activated by SMA wires and applied to manipulator robotic structures or biomimetic actuation modules. The soft beam demonstrates adaptability and opens up additional applications, such as adaptive aerodynamic structures (e.g., morphing wings).

5. ACKNOWLEDGEMENTS

The authors are grateful to Brazilian National Council for Scientific and Technological Development (CNPq) for the scholarship PQ-1C, grant number 302740/2018-0 and the Paraiba State Research Support Foundation (FAPESQ-PB) for the project NISMArt, grant number 044/2023.

6. REFERENCES

Almubarak, Y., Punnoose, M., Maly, N.X., Hamidi, A. and Tadesse, Y., 2020. “Kryptojelly: A jellyfish robot with confined, adjustable pre-stress, and easily replaceable shape memory alloy NiTi actuators”. Smart Materials and Structures, Vol. 29, No. 7, p. 075011.

Antonucci, V. and Martone, A., 2021. “Phenomenology of shape memory alloys”. In Shape memory alloy engineering, Elsevier, pp. 115–139.

Cohades, A. and Michaud, V., 2018. “Shape memory alloys in fibre-reinforced polymer composites”. Advanced Industrial and Engineering Polymer Research, Vol. 1, No. 1, pp. 66–81.

De Araújo, C., Rodrigues, L., Neto, J.C. and Reis, R., 2008. “Fabrication and static characterization of carbon-fiber reinforced polymers with embedded NiTi shape memory wire actuators”. Smart Materials and Structures, Vol. 17, No. 6, p. 065004.

Demers, V., Brailovski, V., Prokoshkin, S. and Inaekyan, K., 2009. “Optimization of the cold rolling processing for continuous manufacturing of nanostructured Ti–Ni shape memory alloys”. Journal of materials processing Technology, Vol. 209, No. 6, pp. 3096–3105.

Granberry, R., Barry, J., Holschuh, B. and Abel, J., 2021. “Kinetically tunable, active auxetic, and variable recruitment active textiles from hierarchical assemblies”. Advanced Materials Technologies, Vol. 6, No. 3, p. 2000825.

Han, M.W., Kim, M.S. and Ahn, S.H., 2020. “Shape memory textile composites with multi-mode actuations for soft morphing skins”. Composites Part B: Engineering, Vol. 198, p. 108170.

Holanda, A.C.C., 2021. Development of a flexible silicone plate with deformation activated by shape memory alloy actuators (in Portuguese). Master’s thesis, Graduate Program in Mechanical Engineering, Federal University of Campina Grande, Campina Grande, Brasil.

Hwang, J. and Wang, W.D., 2022. “Shape memory alloy-based soft amphibious robot capable of seal-inspired locomotion”. Advanced Materials Technologies, Vol. 7, No. 6, p. 2101153.

Jung, W.K., Lee, S.M., Ahn, S.H. and Park, J., 2022. “Development and assessment of a knitted shape memory alloy based multifunctional elbow brace”. Journal of Industrial Textiles, Vol. 51, No. 2_suppl, pp. 1989S–2009S.

Kazemi-Lari, M.A., Dostine, A.D., Zhang, J., Wineman, A.S. and Shaw, J.A., 2019. “Robotic jellyfish actuated with a shape memory alloy spring”. In Bioinspiration, Biomimetics, and Bioreplication IX. SPIE, Vol. 10965, p. 1096504.

Khan, S., Pydi, Y.S., Prabu, S.M., Palani, I. and Singh, P., 2021. “Development and actuation analysis of shape memory alloy reinforced composite fin for aerodynamic application”. Sensors and Actuators A: Physical, Vol. 331, p. 113012.

Kim, M.S., Heo, J.K., Rodrigue, H., Lee, H.T., Pané, S., Han, M.W. and Ahn, S.H., 2023. “Shape memory alloy (SMA) actuators: The role of material, form, and scaling effects”. Advanced Materials, Vol. 35, No. 33, p. 2208517.

Kohl, M. and Kohl, M., 2004. “Shape memory actuation”. Shape Memory Microactuators, pp. 62–95.

Lagoudas, D.C., 2008. Shape memory alloys: modeling and engineering applications. Springer.

Lee, J.H., Chung, Y.S. and Rodrigue, H., 2019. “Long shape memory alloy tendon-based soft robotic actuators and implementation as a soft gripper”. Scientific reports, Vol. 9, No. 1, p. 11251.

Lee, S.M., Jung, W.K., Park, J. and Ahn, S.H., 2022. “Development of a 4d hand gripping aid using a knitted shape memory alloy and evaluation of finger-bending angles in elderly women”. Fashion and Textiles, Vol. 9, No. 1, pp. 1–16.

Miller, D.A. and Lagoudas, D.C., 2000. “Thermomechanical characterization of **N**iTiCu and NiTi SMA actuators: influence of plastic strains”. Smart Materials and Structures, Vol. 9, No. 5, p. 640

Otsuka, K. and Wayman, C.M., 1999. Shape memory materials. Cambridge university press.

Park, S.J. and Park, C.H., 2019. “Suit-type wearable robot powered by shape-memory-alloy-based fabric muscle”. Scientific reports, Vol. 9, No. 1, p. 9157.

Rodrigue, H., Wei, W., Bhandari, B. and Ahn, S.H., 2015. “Fabrication of wrist-like SMA-based actuator by double smart soft composite casting”. Smart Materials and Structures, Vol. 24, No. 12, p. 125003.

Sharifi, E.M., Karimzadeh, F. and Kermanpur, A., 2014. “The effect of cold rolling and annealing on microstructure and tensile properties of the nanostructured Ni50Ti50 shape memory alloy”. Materials Science and Engineering: A, Vol. 607, pp. 33–37.

Smith, C., Villanueva, A., Joshi, K., Tadesse, Y. and Priya, S., 2010. “Working principle of bio-inspired shape memory alloy composite actuators”. Smart Materials and Structures, Vol. 20, No. 1, p. 012001.

Smith, N., Antoun, G., Ellis, A. and Crone, W., 2004. “Improved adhesion between nickel–titanium shape memory alloy and a polymer matrix via silane coupling agents”. Composites Part A: Applied Science and Manufacturing, Vol. 35, No. 11, pp. 1307–1312.

Tsimbo Fokou, M.R., Xia, Q., Jin, H., Xu, M. and Dong, E., 2023. “A soft robotic fish actuated by artificial muscle modules (sorofaam-1)”. Journal of Bionic Engineering, Vol. 20, No. 5, pp. 2030–2043.

Wang, W., Tang, Y. and Li, C., 2021. “Controlling bending deformation of a shape memory alloy-based soft planar gripper to grip deformable objects”. International Journal of Mechanical Sciences, Vol. 193, p. 106181.

Wei, Z., Sandstroröm, R. and Miyazaki, S., 1998. “Shape-memory materials and hybrid composites for smart systems: Part i shape-memory materials”. Journal of materials science, Vol. 33, pp. 3743–3762.

Wu, R., Han, M.W., Lee, G.Y. and Ahn, S.H., 2013. “Woven type smart soft composite beam with in-plane shape retention”. Smart Materials and Structures, Vol. 22, No. 12, p. 125007.

Zheng, W., Wei, K., Zhu, S., Wang, J., Niu, F., Liu, G. and Yang, R., 2022. “Multi-function untethered actuator based on ni-ti alloy and polylactic acid”. Sensors and Actuators A: Physical, Vol. 344, p. 113697.

7. RESPONSIBILITY NOTICE

The authors are the only responsible for the printed material included in this paper.